VOL.40 Nº4 2023
https://doi.org/10.22491/rmct.v40i4.12375.en

Direct energy deposition additive manufacturing (DED-AM) of surfaces with H13 tool steel powder atomized in Brazil

Rafael Ramos[1], Naiara V. Le Sénéchal[1], Helder P. Vicente[2], Paulo P. O. L. Dyer[2], Andersan S. Paula[1] e Getúlio Vasconcelos[2]
[1] Instituto Militar de Engenharia (IME), Graduate Program in Materials Science and Engineering (PPGCEM), Rio de Janeiro, RJ, Brazil
[2] Instituto de Estudos Avançados (IEAv), Division of Photonics, São José dos Campos, SP, Brazil
*ramos_rr@ime.eb.br

Abstract: *H13 steel powder, for the first-time water atomized in a Brazilian company, was deposited by Direct Energy Deposition (DED) additive manufacturing (AM) over a microalloyed hot rolled steel sheet. This study aimed to evaluate microstructural, compositional, and mechanical aspects in the cross-section of the formed deposit layers, as well as at the substrate-first layer interface, using optical and scanning electron microscopy and microhardness analysis. The depositions resulted in a morphology with columnar grains close to the substrate (epitaxial growth) and a reduction in columnar extension, accompanied by changes in microhardness, in reheated areas at the intersections derived from layers stacking, which overlap involved partial layer remelting, and the in situ heat treatment of remelted zones adjacent volume. In addition, adequate geometric and chemical dilution depth at the first layer-substrate interface anchoring the deposit to the substrate was observed.*

KEYWORDS: *Additive Manufacturing; Direct Energy Deposition; H13 Tool Steel; Microstructure; Dilution.*

Resumo: *Pó de aço H13, pela primeira vez atomizado em água em uma empresa brasileira, foi depositado por manufatura aditiva (MA) via deposição por energia direcionada (DED), sobre chapa laminada de aço microligado. Este estudo objetivou avaliar os aspectos microestruturais, composicionais e mecânicos ao longo da seção transversal das camadas de depósitos formadas, como também na interface substrato-primeira camada, por meio de microscopia óptica e eletrônica de varredura, assim como análise da microdureza. As deposições resultaram em uma morfologia com grãos colunares próximo ao substrato (crescimento epitaxial) e uma redução da extensão colunar, acompanhada de mudanças na microdureza, em áreas reaquecidas nas interseções decorrentes do empilhamento de camadas, cuja sobreposição envolveu a refusão parcial, e o tratamento térmico in situ do volume adjacente às zonas refundidas. Adicionalmente, verificou-se uma diluição química e geométrica com profundidade adequada na interface primeira camada-substrato, garantindo a ancoragem do depósito no substrato.*

PALAVRAS-CHAVE: Manufatura Aditiva; Deposição Por Energia Direcionada; Aço Ferramenta H13; Microestrutura; Diluição.

1. Introduction

H13 steel, widely defined in international standards AISI/SAE, whose classification and chemical composition (see Table 1) was adopted by ABNT NBR NM 122-1 [1], is very useful in the manufacture of molds and dies for casting and injection, due to the stability of its properties at high temperature [2, 3, 4]. However, traditional manufacturing methods are time-consuming, expensive [2], and rely on a sequence of several mechanical manufacturing steps and heat treatments [4].

Table 1 - Chemical composition of H13 steel.

	Elements (% by weight)							
	C	**Mn**	**Si**	**Cr**	**Mo**	**V**	**P**	**S**
Min	0.32	0.20	0.80	4.75	1.10	0.80	-	-
Max	0.45	0.50	1.20	5.50	1.75	1.20	0.03	0.03

Source: ABNT NBR NM 122-1 [1].

Additive manufacturing (AM), including directed energy deposition (DED), is gaining the attention of the tooling industry due to its potential to manufacture parts with customized geometries, complex cooling systems, and functionally graded materials (FGM) [2, 5]. Among the AM techniques, DED is capable of producing larger pieces [6] with the use of robotic arms that guarantee freedom of movement in various directions [7]. Nevertheless, understanding the peculiarities of the process and its relationship with the properties of the parts produced is a challenge [2, 7].

Parts produced by DED-AM normally have a cellular structure with equiaxial grains in reheated areas (intersection of layers) and columnar grain morphology in the lower portions (epitaxial growth), because of temperature gradients and heat flow during the process, with different properties associated with each of these regions [3].

The deposition of laterally or vertically overlapped tracks can lead to remelted or at least thermally affected zones (Heat Affected Zones – HAZ), in which heat treatments can occur [8]. In turn, fusion in deposition also generates a layer-layer or layer-substrate dilution depth ensuring the physical bond between them, as well as their chemical interaction. This situation is influenced by the process parameters, the convection in the melt pools, and the solubility between the elements (mainly at the layer-substrate interface) [9].

Thus, this study aimed to evaluate, from the cross-section of samples manufactured by DED-AM with fixed energy density, the interactions between the first layers of a deposit and the substrate.

2. Material and Methods

The material manufactured by DED-AM is a H13 steel powder water atomized, produced in a Brazilian company for the first time, to the best of our knowledge [10]. The material was used in an attempt to stimulate national technological independence and reduce costs, considering the high prices involved in importing such powder manufactured by gas atomization in enterprises abroad.

Before being processed in the DED-AM equipment, the powder was sieved to be between 53 μm and 150 μm (mesh sieves #270 and #100) and had its particles analyzed by micrograph interpretation using ImageJ, generating results of D_{50} = 68 μm and D_{90} = 128 μm. Moreover, the morphology of the powder was irregular, with some spherical particles in the middle of several pear-like ones [11], as illustrated in Figure 1, aspects that apparently did not affect the feed flow or even the densification of the deposition in the DED-AM system.

The depositions were carried out on low carbon steel substrates, with relevant manganese content and molybdenum microaddition (Table 2 [12]), in a manufacturing laboratory of the Institute for Advanced Studies (IEAv), agency of the Aeronautics Technological Center (CTA) and partner in projects of the Military Engineering Institute (IME). A non-proprietary production apparatus was used, illustrated in Figure 2, resulting from the integration of several components whose initial parameterization was discussed in another study [10], which also aimed to stimulate national technological independence.

Figure 1 - SEM micrographs of H13 powder particles: (A) SE detector; (B) BSE detector.

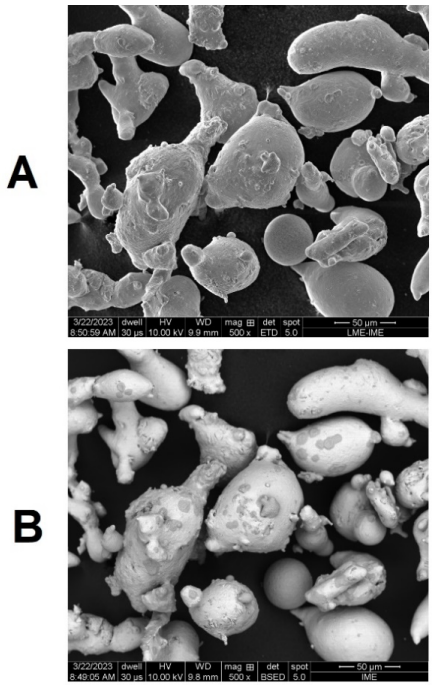

Source: The author.

Table 2 - Chemical composition of the steel used as substrate.

Elements (% by weight)							
C	**Mn**	**P**	**S**	**Si**	**Cu**	**Ni**	**Cr**
0.082	1.606	0.016	0.008	0.005	0.014	0.009	0.020
Mo	**Sn**	**Al**	**N**	**Ti**	**Nb**	**V**	**B**
0.155	0.003	0.028	0.006	0.002	0.014	0.005	0.000

Source: Souza (2011) [12].

The metallic powder was conducted by inert argon gas (flow of 6 L/min, feed rate of 7.2 g/min) and melted by a laser beam (1282.5 W power and 5 mm/s scanning speed) during deposition, generating the superposition of several tracks and allowing the manufacture of samples with surfaces of one, two, and three layers stacked on the substrate, as illustrated in Figure 3. The mentioned parameters were defined after several tests with various combinations between scanning speeds, laser powers, and powder feed rates, among others [10].

Figure 2 - Overview of deposition equipment: (A) robotic arm; and (B) laser head and powder feeders.

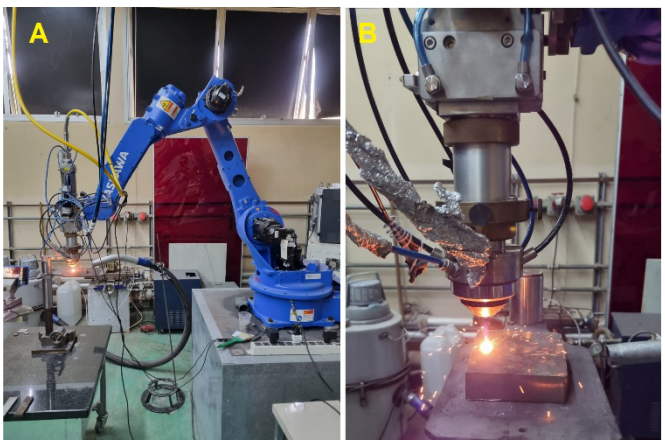

Source: The author.

The samples were cross-sectioned, as illustrated in Figure 4, prepared (sanded, polished, and chemically attacked with reagents Villela and Nital 5%), and evaluated by optical microscopy (OM) and scanning electron microscopy (SEM), the latter associated with the use of secondary (SE) and backscattered electron detectors (BSE), in addition to energy dispersive X-ray spectroscopy (EDS). Vickers microhardness tests were also performed (HV, 200 gf load, 3 to 5 indentations per horizontal line). The images from the SEM micrographies of the metal powder and the cross sections of the depositions were analyzed in the ImageJ software for particle size distribution and thickness, respectively.

Figure 3 - Schematic diagram of the depositions performed.

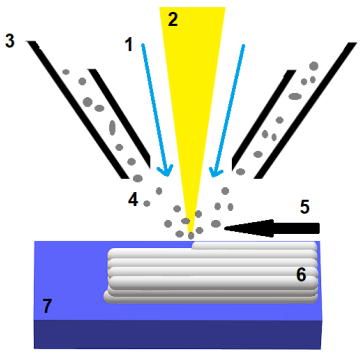

Item	Description
1	Protection gas
2	Laser beam
3	Head structure
4	H13 metallic powder
5	Scanning direction
6	Deposited tracks
7	Substrate

Source: The author.

Figure 4 - View of the cut made in the deposited samples: (A) schematic drawing; and (B) samples with one, two, and three layers after cutting and embedding.

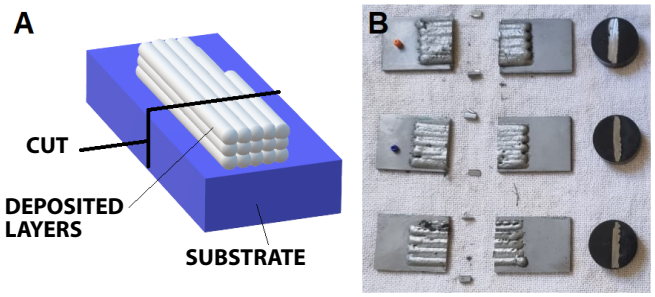

Source: The author.

3. Results

Micrographs resulting from the OM analysis of the cross section of the depositions with one, two, and three layers were evaluated. Figure 4B hows three distinct depositions, and the areas in which the interaction between deposit and substrate or between layers was clear were chosen for micrographic analysis.

Figure 5 presents the dilution zone (DZ) between the deposited layers and the substrate, a region delimited by dashed lines with orientation close to horizontal, deflecting to follow the contour of the deposit bead observed, revealing a good level of anchoring and densification. Furthermore, the emergence of microstructural transition zones is visible in Figures 5B and 5C, compared to 5A. These heat affected zones (HAZ) occur due to the heat supply resulting from the deposition of laterally adjacent or overlapping tracks, in which the columnar aspect is reduced due to *in situ* heat treatments [5, 8].

In Figure 6, with a slightly higher magnification, the columnar aspect of the grains near the deposit-substrate interface, resulting from epitaxial growth, becomes even clearer than in Figure 5. In both cases, with indicative lines tending to be vertically oriented, remembering that there is no intention to demarcate all existing contours. Furthermore, when comparing the three depositions, one can notice the reduction of the columnar morphology of the grains, as well as their coalescence in samples with more layers of deposits and the predominance of the columnar aspect in higher positions (as in Figure 6C), in which new layers were deposited. Such changes are attributed to the greater heat flow in depositions with more layers, to the fact that the lower layers are already deposited and susceptible to the thermal action of the subsequent depositions and, finally, to the fact that such thermal action generates locally heterogeneous microstructures in the AM, depending on the thermal cycle developed in each position [13].

Figure 5 - Micrographs obtained via OM, bright field. Deposited layers: A, one; B, two; and C, three.

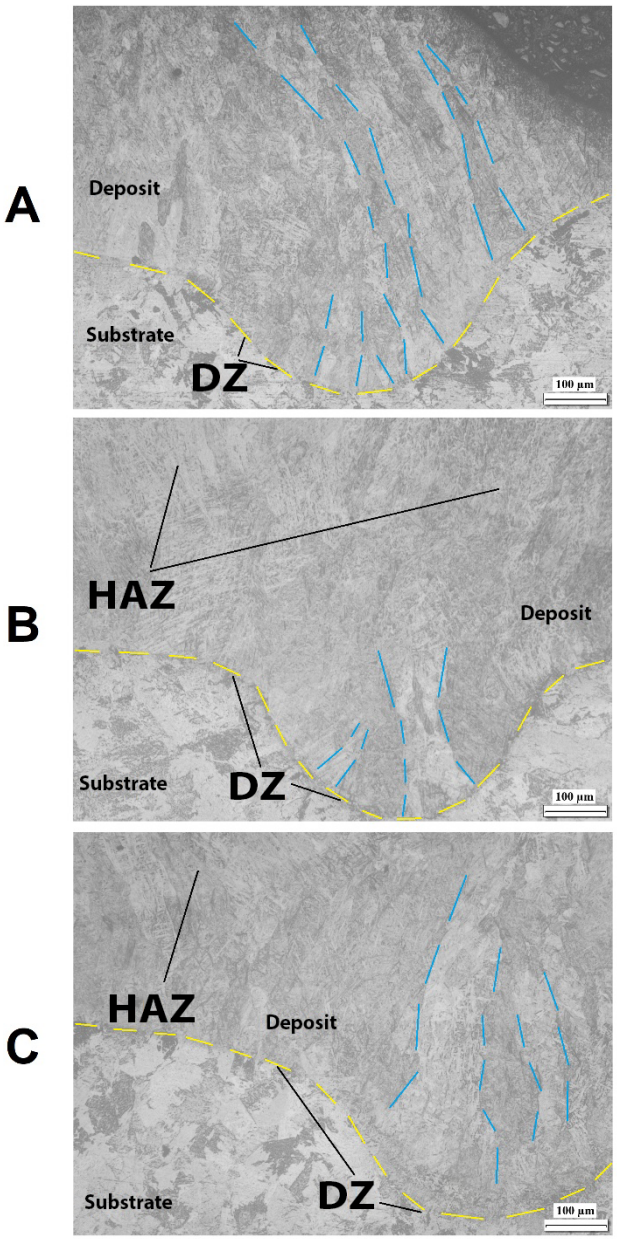

Source: The author.

In turn, the observation by dark field OM is shown in Figure 7, reinforcing the visualization of the columnar microstructure of the grains already mentioned (A) and the occurrence of thermal effects between adjacent layers; in (B), the upper portion of the bead of the first layer presents some morphological changes; in (C), the transition zone between the second

and third layers appears in the sample in which three layers were deposited. In Figure 7C, the change in the direction of grain growth in the microstructure is also noticeable, as a result of changes in the heat flow due to the deposition of layers higher than previously deposited, since the grains grow in the opposite direction to the thermal gradient present in the solidifying melt pool [14].

Figure 6 - Micrographs obtained via OM, bright field, high magnification. Deposited layers: A, one; B, two; and C, three.

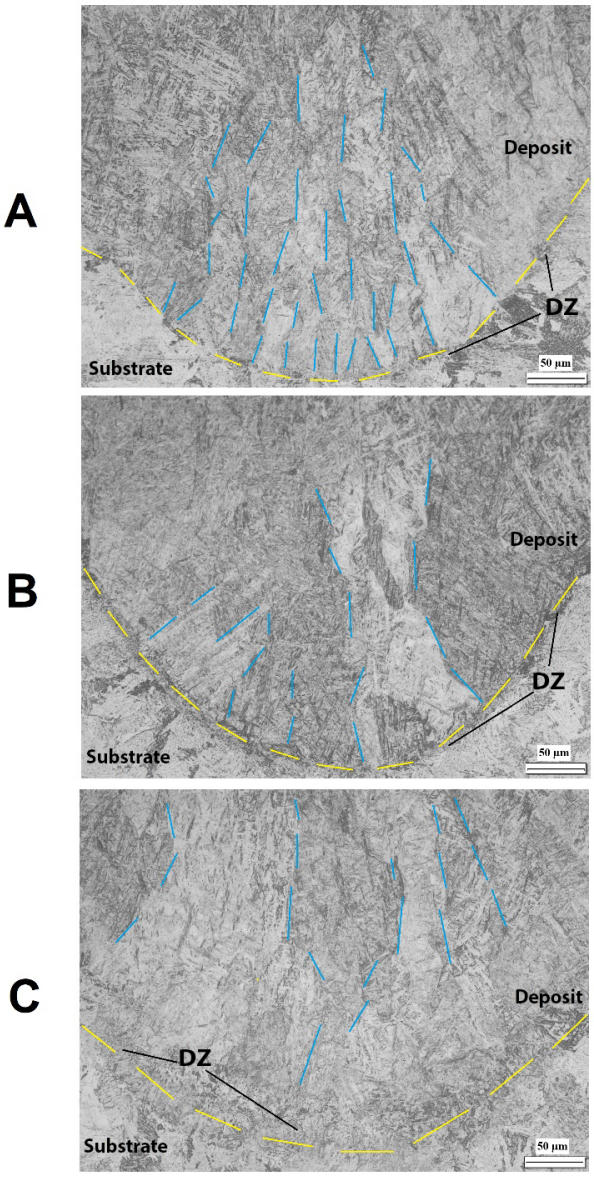

Source: The author.

In the micrographs obtained via SEM with low magnification (Figure 8), it is possible to confirm the fact that the solidification is guided by the heat flow [14] and thus is modified by the number of layers and deposition strategy, as indicated by auxiliary lines marked with stars, drawn on the images following the direction of the solidification front in the microstructure. In addition, a good level of densification and anchoring in the substrate is confirmed, despite the presence of a few pores (Figures 8A and 8B). No evidence of the balling defect [6] was found, which had been observed in previous studies with the metal powder and the productive apparatus used, but in other configurations [10], indicating an improvement in the selection of the productive parameters used.

Figure 7 - Micrographs obtained via OM, dark field. Deposited layers: A, one; B, two; and C, three.

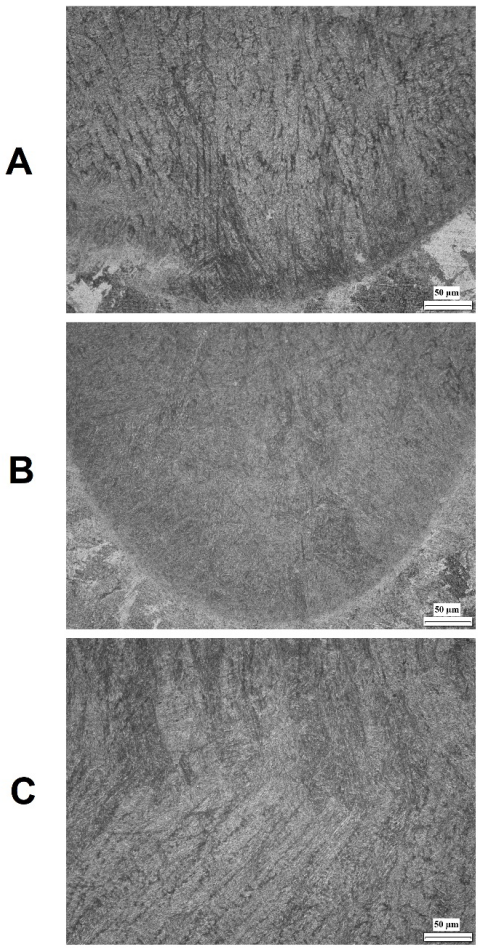

Source: The author.

Another aspect visible in Figure 8 is the existence of regions of greater penetration of the deposit on the substrate forming the already mentioned beads, regions related to the central portion of the laser beam during scanning, whose thermal action gradually decreases in positions that distance themselves from this central line.

Figure 8 - Micrographs obtained via SEM, low magnification. Deposited layers: A, one; B, two; and C, three.

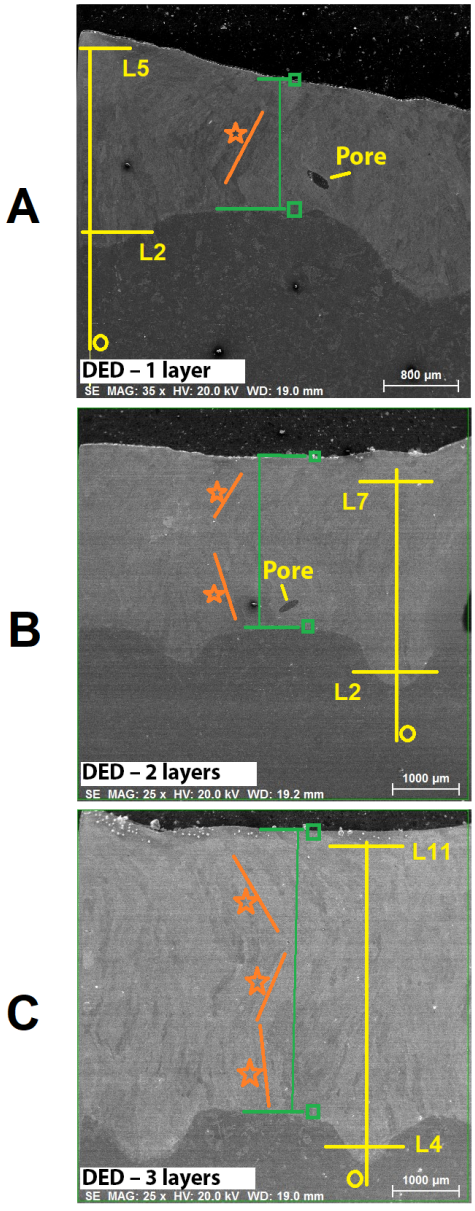

Source: The author.

Figure 8 also shows, by marking a small circle at the base, vertical lines cut by horizontal lines with indications of numbers and letters (L2 and L5 in 8A; L2 and L7 in 8B; and L4 and L11 in 8C). They serve as a reference for a study of Vickers microhardness along the vertical profile of each sample under study, which will be presented below, highlighting that measurements were made on horizontal levels 0.5 mm apart from each other, starting at line 1, in position totally belonging to the substrate (L1, not shown). The lines represented in Figure 8 refer to the horizontal profiles in which the indentations began to occur in regions of the deposits (L2 in A and B and L4 in C), as well as to the final positions of greater height evaluated in the region of the deposits (L5 in A; L7 in B; and L11 in C).

Moreover, the micrographs presented in Figure 8 were treated using the ImageJ software, allowing us to estimate the growth of the layers as having 1.51 mm in the sample with one layer, 2.55 mm in the sample with two, and 4.22 mm in the deposition with three layers (respectively in Figures 8A, 8B, and 8C). Such measurements were made from the region between two beads to the upper surface of the deposit, which are identified by horizontal lines, accompanied by squares, represented in the images of Figure 8. We highlight that we aimed to evaluate the estimated growth of the deposit and show that the increase in the number of layers deposited, with the parameters used, resulted in an effective growth of the deposit. The definition of a more representative value of the total deposit thickness would require a greater number of measurements, with images of different regions, given the possibility of variation in deposit thickness in different regions, aspects that were not the subject of this study.

An elemental chemical mapping in a microarea by EDS/SEM was conducted to distinguish the regions of the substrate and the deposit, as well as to identify the extent of the dilution zone, a region in which the mixture of alloying elements of the substrate and the deposit is expected. Given these objectives, although there are other alloying elements in these two portions under study, the alloying elements Cr and Mn were chosen for observation, because their compositions stand out, in percentage terms, in the deposit

(Cr, approximately 5%) and in the substrate (Mn, approximately 1.6%), with a small participation in the other portion (Cr 0.02% in the substrate; expected Mn of about 0.35% in the deposit), as can be seen in Tables 1 and 2, a contrast that allowed a better distinction between deposit and substrate.

The results of the chemical mapping by EDS are presented in Figure 9, indicating the existence of well-defined domains for the two portions of the material (substrate and deposit) and showing that the dilution region was not extensive, as well as confirming an adequate penetration of the deposit on the substrate.

Figure 9 - Mapping of areas by EDS. Deposited layers: A, one; B, two; and C, three.

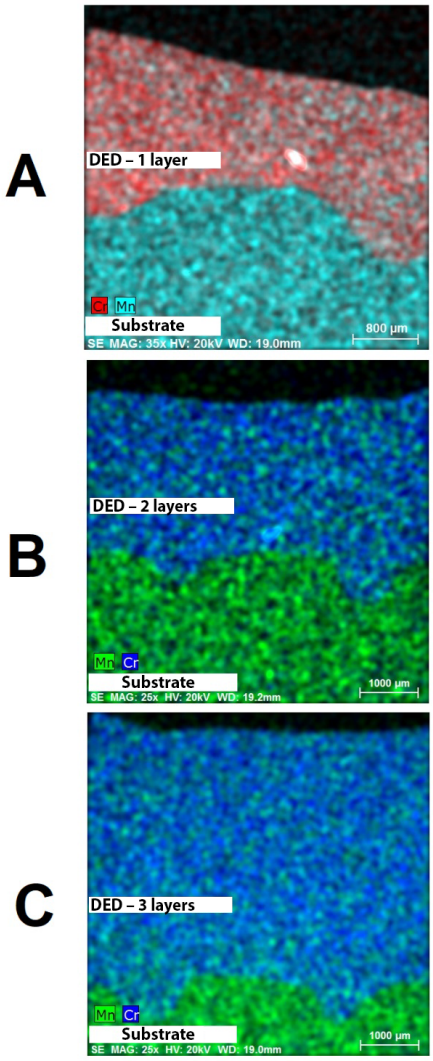

Source: The author.

An elemental chemical mapping by EDS/SEM was also performed (Figure 10), starting from the deposit towards the substrate, which confirmed the existence of two domains with relatively homogeneous chemical composition (deposit and substrate), separated by a transition portion in which the chemical composition changed smoothly. This revealed a good level of chemical dilution, in addition to confirming that such chemical mixing occurred to a limited extent [15], and this pattern was observed in all three conditions under study. Furthermore, the elemental mappings (Figure 10) revealed the evolution of the other alloying elements not selected in the microareas mappings of Figure 9, in addition to corroborating the already mentioned idea that Cr and Mn were able to indicate the regions of each of the domains (deposit and substrate) and the transition zone between them.

Figure 10 - Elemental mapping by EDS. Deposited layers: A, one; B, two; and C, three.

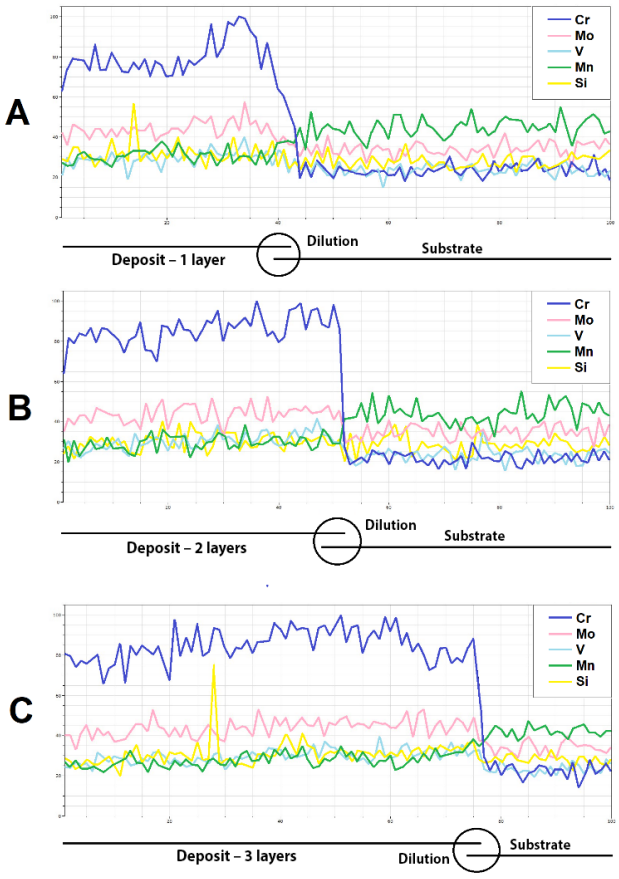

Source: The author.

Finally, the analysis with Vickers microhardness (HV) test, following the vertical profiles already mentioned, identified in Figure 8 by the vertical lines with circle marking at their base, can be seen in Figure 11, in which the mean values of HV and the standard deviations (SD) for each of the horizontal lines along the vertical profiles already mentioned are presented. An increase in HV is observed in the direction from the substrate towards the upper portions of the H13 deposit, despite a slight reduction in HV values in some measurement lines, and the SD is a tool to observe how the properties differ in adjacent regions due to the thermal influence of the sequential deposition of tracks [2, 3], above or laterally, as well as the regions influenced by dilution. In addition, large SD values marked the line where the deposits began, as they referred to the lines with indentations in the region of penetration of the deposit into the substrate (beads), already mentioned), as well as in the substrate portions adjacent to the beads (L2, L2, and L4, respectively, in Figures 11A, 11B, and 11C, also illustrated in Figure 8).

4. Conclusions

H13 deposits containing one, two, and three layers showed a good level of anchoring and interaction with the substrate, as well as spatially limited dilution regions with smooth transition of chemical composition at the substrate-deposit interface.

In addition, there was a directional development of the microstructure after solidification, related to the epitaxial growth of the columnar grains and the heat flow throughout the solidification of the layers. Moreover, the thermal influence of laterally adjacent or overlapped tracks was portrayed in the variation of microhardness values along the vertical profile and also in the same horizontal line, as well as in the changes in microstructure morphology, confirming a heterogeneous pattern of microstructure and properties in samples "as manufactured" by AM.

This study opens space for a continuation by similar analysis, but with samples submitted to heat treatment routes, seeking to homogenize microstructure and properties throughout the deposited material.

Acknowledgements

The authors thank: Villares Metals, for offering conventional H13 steel, which was atomized; IEAv and IME, for the production structure and characterization of materials; the Brazilian Center for Physical Research (CBPF), for support in cutting and preparation of substrates; the Brazilian Funding Agency for Studies and Projects (FINEP) and the Brazilian Federal Agency for Support and Evaluation of Graduate Education (CAPES) (Pró-Defesa IV and PROEX), for the financial support.

Figure 11 - Mean results of Vickers microhardness (HV) and its standard deviations (SD). Deposited layers: A, one; B, two; and C, three.

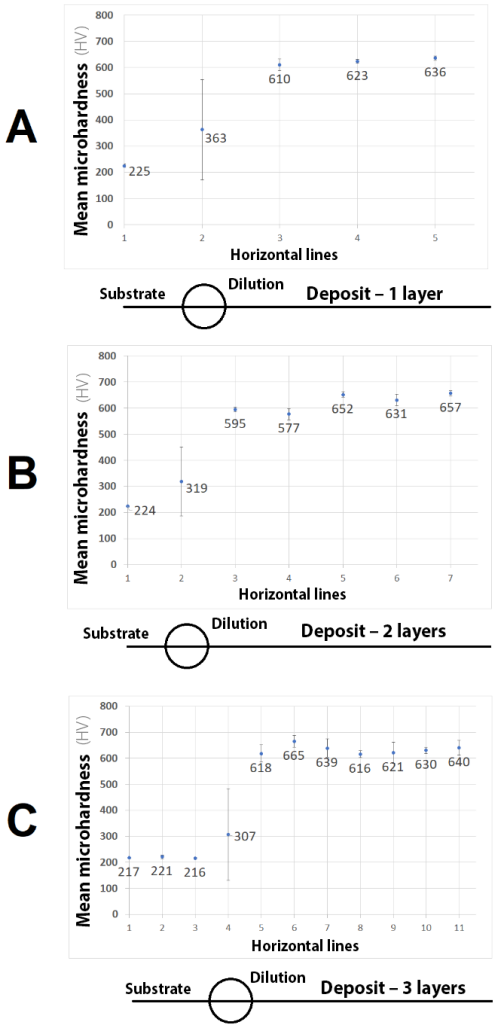

Source: The author.

References

[1] ASSOCIAÇÃO BRASILEIRA DE NORMAS TÉCNICAS. **NBR NM 122-1**: Aços ferramentas – parte 1: Classificação, designação e composição química. Rio de Janeiro: ABNT, 2005.

[2] ZHAO, X. *et al*. The effect of thermal cycling on direct laser-deposited gradient H13 tool steel: Microstructure evolution, nanoprecipitation behavior, and mechanical properties. **Materials Today Communications**, [*s. l.*], v. 25, 101390, 2020.

[3] JOSHI, S. *et al*. Solidification and microstructure evolution in additively manufactured H13 steel via directed energy deposition: Integrated experimental and computational approach. **Journal of Manufacturing Processes**, Amsterdam, v. 68, p. 852-866, 2021.

[4] KANG, M. *et al*. The effects of annealing temperature and cooling rate on carbide precipitation behavior in H13 hot-work tool steel. **Journal of Alloys and Compounds**, Amsterdam, v. 627, p. 359-366, 2015.

[5] BOHLEN, A. *et al*. Additive manufacturing of tool steel by laser metal deposition. **Procedia Cirp**, Amsterdam, v. 74, p. 192-195, 2018.

[6] DEBROY, T. *et al*. Additive manufacturing of metallic components–process, structure and properties. **Progress in Materials Science**, Amsterdam, v. 92, p. 112-224, 2018.

[7] LIMA, M. S. F. Processo de AM por adição de lâminas, por deposição com energia direcionada e híbridos. *In*: VOLPATO, N. (org.). **Manufatura Aditiva**: Tecnologias e Aplicações da Impressão 3D. São Paulo: Blücher, 2017. p. 271-287.

[8] AMIRABDOLLAHIAN, S. *et al*. Tempering behavior of a direct laser deposited hot work tool steel: Influence of quenching on secondary hardening and microstructure. **Materials Science and Engineering: A**, Amsterdam, v. 814, 141126, 2021.

[9] PELLIZZARI, M. *et al*. Optimizing direct laser metal deposition of H13 cladding on CuBe alloy substrate. **Surface & Coatings Technology**, Amsterdam, v. 432, 128084, 2022.

[10] RAMOS, R. *et al*. Parametrização de equipamento de deposição por energia direcionada utilizando pó de aço ferramenta H13 atomizado em água. *In*: CONGRESSO ANUAL DA ABM, 76., 2023, São Paulo. **Anais** […]. [*S. l.*]: ABM, 2023. p. 2473-2483. DOI: 10.5151/2594-5327-39934.

[11] BRAGA, V. *et al*. Microstructural and mechanical aspects of laser metal deposited H13 powder for die repair. **Materials Today Communications**, Amsterdam, v. 29, 102945, 2021.

[12] SOUZA, A. C. A. **Produtos de transformações de fases obtidos sobre distintas condições de resfriamento em aço baixo carbono com microadição de molibdênio laminado a quente**. 2011. Projeto de Conclusão de Curso (Graduação) – Universidade Federal Fluminense, Volta Redonda, 2011.

[13] GE, J. *et al*. Investigation on H13 buildups produced with wire arc additive manufacturing: Deposition strategies-induced microstructural evolution and mechanical performances. **Journal of Alloys and Compounds**, Amsterdam, v. 860, 157893, 2021.

[14] YANG, X. *et al*. Microstructure evolution and mechanical properties of H13 steel produced by Selective Electron Beam Melting. **Materials Characterization**, Amsterdam, v. 203, 113053, 2023.

[15] DASS, A.; MORIDI, A. State of the art in directed energy deposition: From additive manufacturing to materials design. **Coatings**, Basel, v. 9, n. 7, n. 418, 2019.